1 Summertime response of ozone and fine particulate
2 matter to mixing layer meteorology over the North
3 China Plain

4 Jiaqi Wang[1], Jian Gao[1], Fei Che[1], Xin Yang[1], Yuanqin Yang[2], Lei Liu[2], Yan Xiang[3]

5 [1]State Key Laboratory of Environmental Criteria and Risk Assessment, Chinese Research Academy of
6 Environmental Sciences, Beijing 100012, China

7 [2]State Key Laboratory of Severe Weather and Key Laboratory for Atmospheric Chemistry of CMA,
8 Chinese Academy of Meteorological Sciences, Beijing 100081, China

9 [3]Institutes of Physical Science and Information Technology, Anhui University, Hefei, China

10 *Correspondence to:* Jian Gao (gaojian@craes.org.cn)

11 **Abstract.** Measurements of surface ozone (O_3), $PM_{2.5}$ and its major secondary components (SO_4^{2-},

12 NO_3^-, NH_4^+, and OC), mixing layer height (MLH) and other meteorological parameters were made in

13 the North China Plain (NCP) during warm seasons (June–July) in 2021. The observation results

14 showed that the summertime regional MDA8 O_3 initially increased and reached the maximum (158.47

15 $\mu g\ m^{-3}$) when MLH at around 900–1200 m, then turned to decrease with further evolution of MLH.

16 Interestingly, synchronized increases in $PM_{2.5}$ concentration along with the development of the mixing

17 layer (MLH < 1200 m) have been witnessed, and the positive response of $PM_{2.5}$ to MLH was

18 significantly associated with the increase in SO_4^{2-} and OC. It was found that this increasing trend of

19 $PM_{2.5}$ with elevated MLH was not only determined by the effect of wet deposition process but also by

20 the enhanced secondary chemical formation, which was related to appropriate meteorological

21 conditions (50 % < RH < 70 %) and increased availability of atmospheric oxidants. Air temperature

22 played a minor role in the change characteristics of $PM_{2.5}$ concentration, but greatly controlled the

23 competing role of SO_4^{2-} and NO_3^-. The concentrations of SO_4^{2-} and OC increased synchronously with

24 elevated MDA8 O_3 concentration, and the initial increase of $PM_{2.5}$ along with the increased MLH

25 corresponded well with that of MDA8 O_3. We highlight that the correlation between MLH and

26 secondary air pollutants should be treated with care in hot seasons, and the impact of atmospheric

27 oxidation capacity on surface $PM_{2.5}$ change profile along with the evolution of mixing layer should be

28 considered when developing $PM_{2.5}$-O_3 coordinated control strategies.

29

30
31
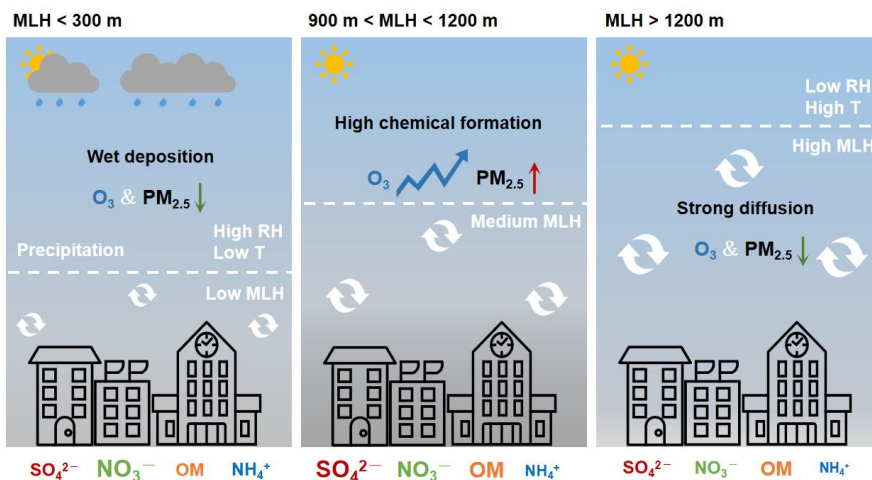
1 Introduction

Surface ozone (O_3) and $PM_{2.5}$ (atmospheric fine particles with an aerodynamic diameter of less than 2.5 μm) are important air pollutants in the atmosphere and have aroused a lot of attention from the public due to their adverse health impact (Jiang et al., 2018; Cohen et al., 2017; Gao and Ji, 2018). Even though stringent clean air actions have been implemented in China during the past decade, high concentrations of O_3 and/or $PM_{2.5}$ exceeding the national air quality standards still occurred during warm seasons (June–August) in China, especially in the North China Plain (NCP), the economic center of China (Dai et al., 2023). O_3 is a secondary pollutant originated from photochemical oxidation of volatile organic compounds (VOC) and carbon monoxide (CO) in the presence of nitrogen oxides (NO_X), and $PM_{2.5}$ is mainly determined by the atmospheric processes of emissions and secondary formation from gaseous precursors. In addition to air pollutant emissions, meteorological conditions play critical roles in the formation of $PM_{2.5}$ and O_3 (Miao et al., 2021). Mixing layer height (MLH), which influences the vertical mixing within the pollution mixing layer and determines the dilution of pollutants emitted near the ground (Haman et al., 2014; Zhu et al., 2018; Lou et al., 2019), often serves as a critical physical parameter in atmospheric environmental evaluation. Elucidating the association of MLH with surface O_3 and $PM_{2.5}$ is fundamental for the development of $PM_{2.5}$-O_3 coordinated control strategies.

The response of air pollution to MLH was changeable and complicated (Miao et al., 2021). Previous works frequently assumed that the narrowing of mixing layer resulted in accumulation of pollutants near the ground and the increase in MLH was expected to reduce $PM_{2.5}$ concentration due to dilution (Murthy et al., 2020; Du et al., 2013). However, the relationship between mixing layer structure and $PM_{2.5}$ concentration depends on the site, observation period, and the properties of MLH retrievals (Geiß et al., 2017). Even though the link between $PM_{2.5}$ concentrations and MLH has been investigated in many studies, most observations were conducted in winter conditions and few studies in hot seasons. Interestingly, in some cities, such as Delhi (Murthy et al., 2020) and Shanghai (Pan et al., 2019; Miao et al., 2021), the increase in $PM_{2.5}$ has been observed when MLH increased during summertime. As for O_3, the relationship between the changes in the MLH and O_3 concentrations is very complex. Both increase or decrease of O_3 has been observed corresponded to the growth of MLH. To first order, O_3 concentration decreases along with the increase of MLH owing to dilution. Second, an

61 increase in MLH generally promotes the downward mixing of upper air containing higher O_3 (Ma et al.,

62 2021; Haman et al., 2014; Xu et al., 2018). In addition, the meteorological conditions along with the

63 changes of MLH can influence O_3 concentrations through effecting O_3 gaseous precursors or

64 production rates (Porter and Heald, 2019; Zhang et al., 2022). The combined effects of these processes

65 ultimately determine whether O_3 decreases or increases.

66 Other meteorological variables in the mixing layer were also found to significantly affect $PM_{2.5}$

67 and O_3 concentrations. The poor air quality in the NCP was tightly associated with near-surface

68 southerly winds and warm stagnant conditions during summertime (Zhang et al., 2015a). The increase

69 in $PM_{2.5}$ concentration often coincided with high relative humidity (RH) conditions (Liu et al., 2017b),

70 which was beneficial to liquid-phase heterogeneous reactions and fine particle hygroscopic growth

71 (Seinfeld and Pandis, 2006; Wang et al., 2016; Zhang et al., 2015b). Temperature was essential to

72 secondary chemical reaction (Dawson et al., 2007). The increase in temperature can promote chemical

73 reaction rates, but also stimulate the evaporation of semi-volatile aerosol components, such as nitrate

74 (Wen et al., 2018). For O_3, elevated O_3 concentrations generally happened on days with strong sunlight

75 and low wind speeds, which favored the photochemical production and the accumulation of O_3 and its

76 precursors. Several studies have shown that O_3 was significantly positive correlated with temperature,

77 but negatively correlated with RH (Li et al., 2021; Hou and Wu, 2016; Steiner et al., 2010).

78 Secondary $PM_{2.5}$ species, e.g., sulfate (SO_4^{2-}), nitrate (NO_3^-), ammonium (NH_4^+), and organic

79 matter (OM), have increased dramatically in recent years (Cheng et al., 2019; Wang et al., 2022b), and

80 the correlation between O_3 and $PM_{2.5}$ tended to change from negative to positive from 2013 to 2018 in

81 China (Chu et al., 2020). Previous studies have reported that the increased O_3 concentration may cause

82 the enhancement of atmospheric oxidation capacity, thus influencing the chemical compositions,

83 formation pathways, and evolution processes of $PM_{2.5}$ (Cheng et al., 2019; Kang et al., 2021). Even

84 though some studies have discussed the correlations between MLH and some secondary pollutants, the

85 understanding of the interaction between O_3 and $PM_{2.5}$ (including its major components) along with the

86 evolution of mixing layer during warm seasons remained poor owing to the limited observations of

87 $PM_{2.5}$ chemical species involved. The regional-scale observation can represent the variation

88 characteristics for this area and avoid the spatial heterogeneity between the sites. However, to the best

89 of our knowledge, previous observational studies were mostly limited to specific cities. Therefore, it's

90 encouraged to analyze multiple data sources to determine overall trends rather than making conclusions

91 based on a single dataset.

92   To enhance the understanding of the linkages between mixing layer structure and air pollution, in

93 this study, a regional-scale field observation of meteorological factors, O_3, $PM_{2.5}$ concentration and its

94 secondary composition were conducted in the North China Plain (NCP) during a period of severe

95 photochemical pollution (June–July) in 2021. For the first time, the potential association among

96 ground-level observed O_3, $PM_{2.5}$ and its dominant components, and mixing layer meteorological

97 conditions will be explored in the NCP during summertime.

98 **2 Data and methods**

99 **2.1 Measurements**
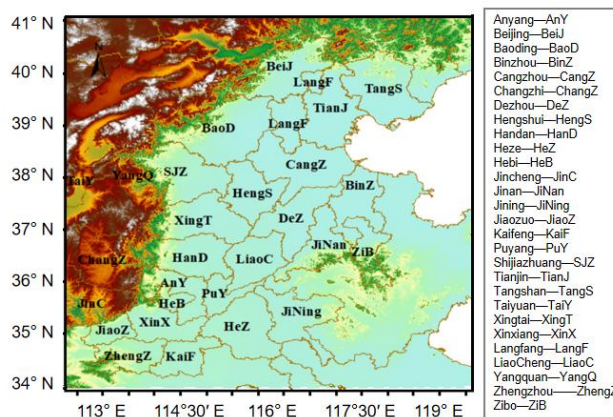
100

101 **Figure 1.** Location of monitoring stations in the NCP.

102   In this study, observation was made in the North China Plain (NCP) from June 1 to July 31, 2021.

103 The air pollution observation stations in the NCP covered two megacities (BeiJ and TianJ) and 26

104 surrounding cities. The geographic locations of these stations are marked in Figure 1. The ground-level

105 O_3, $PM_{2.5}$ and its major components (SO_4^{2-}, NO_3^-, NH_4^+, and OC), and meteorological variables were

106 obtained from the platform of National Atmospheric Particulate Chemical-Speciation-Network, which

107 is established for improving the understanding of the heavy pollution formation mechanism in the NCP

108 and supporting the decision-making of local governments and state administration. Near-ground

109 meteorological variables included the relative humidity (RH), wind speed (WS), temperature, air

110 pressure and daily accumulated precipitation. Mass concentrations of SO_4^{2-}, NO_3^-, and NH_4^+ in $PM_{2.5}$

111 were continuously measured at a 1-h resolution by MARGA (model ADI 2080) or AIM-IC (URG

112   9000D) equipped with a PM$_{2.5}$ sampling inlet. Organic carbon (OC) was measured online by Sunset

113   Semi-Continuous Carbon Analyzer (Sunset Laboratory Inc, USA). PM$_{2.5}$, O$_3$, and other gaseous

114   pollutants, such as NO$_2$ and SO$_2$, were recorded hourly, mainly based on Thermo Scientific samplers

115   and analyzers. Detailed descriptions of these online sampling instruments can be found in our previous

116   works (Kong et al., 2018; Liu et al., 2017a; Pang et al., 2020; Wang et al., 2022b). In this work, O$_3$

117   concentration was characterized by the daily maximum 8-h average (MDA8), and the other pollutants

118   were obtained and recorded by the daily mean in each site to avoid the effect of diurnal variability. The

119   vertical profiles of O$_3$ and aerosol characteristics in BeiJ, SJZ and TangS were measured by the DIAL

120   system, which was developed by the Anhui Institute of Optics and Fine Mechanics (Chinese Academy

121   of Sciences). The overall structure of the DIAL consists of three systems: a emitting system, a

122   receiving system, and a data acquisition system, and the detail information can be found in the work by

123   Wang et al. (2021).

124   **2.2 The calculation of mixing layer heights**

125   From the perspective of atmospheric turbulent motion, the height of the interface, where

126   turbulence is discontinuous, is usually referred to as the mixing layer height (MLH; Stull, 1988). MLH

127   can not be obtained through conventional surface meteorological observations, and it is necessary to

128   use meteorological elements, such as temperature, RH, and air pressure for diagnosis. However, owing

129   to the difficulty in obtaining the vertical distribution of turbulent parameters, in practical applications,

130   MLH is usually determined from the thermal and dynamic effects reflecting turbulent motion. The

131   work by Wang et al. (2022c) has pointed out that the lifting condensation level (LCL) satisfying the

132   supersaturated state can be approximated to MLH. According to the method proposed by Wang et al.

133   (2017), MLH is calculated based on the following equation and represented by air pressure (p):

134    $$\mathrm{MLH} \approx \mathrm{LCL} = 6.11 \times 10^2 \times \left(\frac{0.622 + 0.622\frac{e_s}{p - e_s}}{0.622\frac{e_s}{p - e_s}} \right), \tag{1}$$

135    $$e_s = 6.22 \times \exp\frac{17.13(T - 273.16)}{T - 38}, \tag{2}$$

136   where e_s represents saturated water vapor pressure, T is temperature (K). According to the relationship

137   between air pressure and height, the units of MLH can be converted to the height expression in meters:

138    $$\int_{p_0}^{p_z} dp = -\int_0^z \rho_0 g\, dz, \tag{3}$$

139   where z is the height, ρ_0 is the density of gas, p_z and p_0 represent the air pressure in the height of z and

140   0, respectively.

3 Results and discussions

3.1 General characteristics
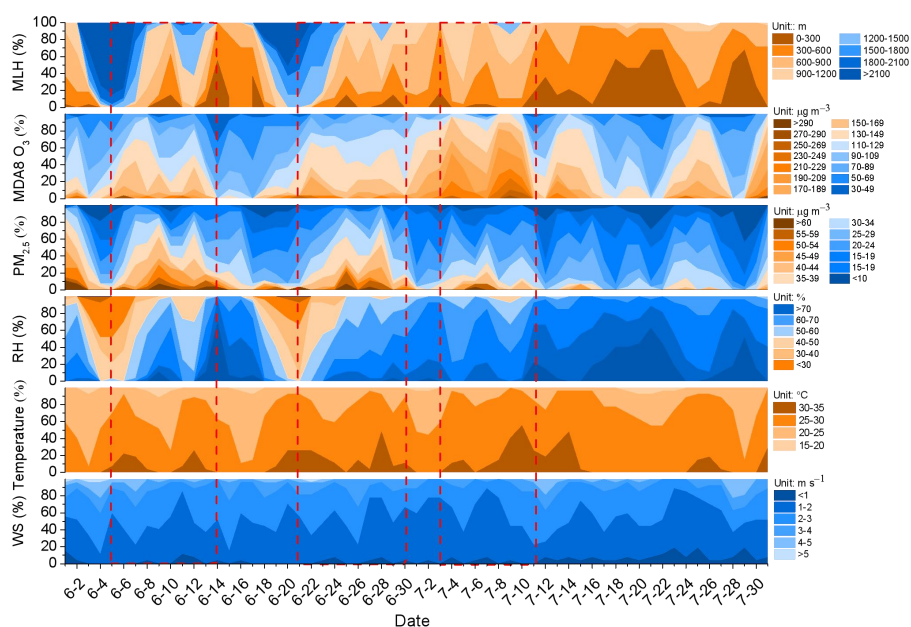
Figure 2. The frequency (%, ratio of occurrence cities to total NCP cities) of PM$_{2.5}$, MAD8 O$_3$, and meteorological factors in the NCP from June 1 to July 31, 2021. The color shading represents different categories classified by PM$_{2.5}$, MDA8 O$_3$, and meteorological factors. The red dash boxes represent three typical PM$_{2.5}$ and O$_3$ pollution episodes.

The summertime change characteristics of ground-level meteorological factors (MLH, RH, temperature, and WS), MDA8 O$_3$, PM$_{2.5}$ and its major components in the NCP were demonstrated in Figure 2 and Figure S1. From June 1 to July 31, 2021, regional PM$_{2.5}$ pollution processes corresponded well with the increasing processes of MDA8 O$_3$, and three concurring PM$_{2.5}$ and O$_3$ pollution episodes have happened: June 5–14 (Episode I), June 21–30 (Episode II), and July 3–11 (Episode III), 2021. During the observation period, the change characteristics of PM$_{2.5}$ and MDA8 O$_3$ concentrations were closely related to the evolution of mixing layer and associated meteorological conditions. Along with the reduction of MLH in Episode I and II, regional MDA8 O$_3$ and PM$_{2.5}$ concentration both gradually climbed up. When MLH fell in the range of 900–1500 m, MDA8 O$_3$ concentration reached the

157   maximum with about 60 % areas higher than 130 μg m^{-3}. When MLH further decreased, MDA8 O$_3$

158   turned to decline, while PM$_{2.5}$ continued to increase until regional MLH lower than 600 m. In Episode

159   III, the MLH in most cities was around 600–1200 m, and the regional MDA8 O$_3$ pollution conditions

160   were much serious than other episodes, with 80 % MDA8 O$_3$ values higher than 150 μg m^{-3}. Generally,

161   the concentration peaks of PM$_{2.5}$ lagged behind that of MDA8 O$_3$ along with the reduction of MLH.

162   Besides, we found that the change characteristics of SO$_4^{2-}$ and NO$_3^-$ were different (Figure S1), and the

163   regional peaks of these two components were inconsistent, especially in Episode II. With the evolution

164   of MLH, NO$_3^-$ climbed up and peaked in June 24 when regional MLH lower that 900 m, while SO$_4^{2-}$

165   reached the maximum in June 28 when MLH was around 900–1500 m. This may be related to other

166   synchronized mixing layer meteorology factors, such as RH and temperature. For example, the

167   evolution of mixing layer often accompanied with changes in temperature. The increase in temperature

168   can promote the chemical formation rate of these secondary components, but also stimulate the

169   volatilization of NO$_3^-$ to gaseous state (HNO$_3$) and lead to the decrease in NO$_3^-$ concentration. Further

170   analysis about the response of O$_3$, PM$_{2.5}$ and its secondary components to different mixing layer

171   meteorology factors will be conducted in the following sections.

172   **3.2 Evolution of ozone with mixing layer meteorology**
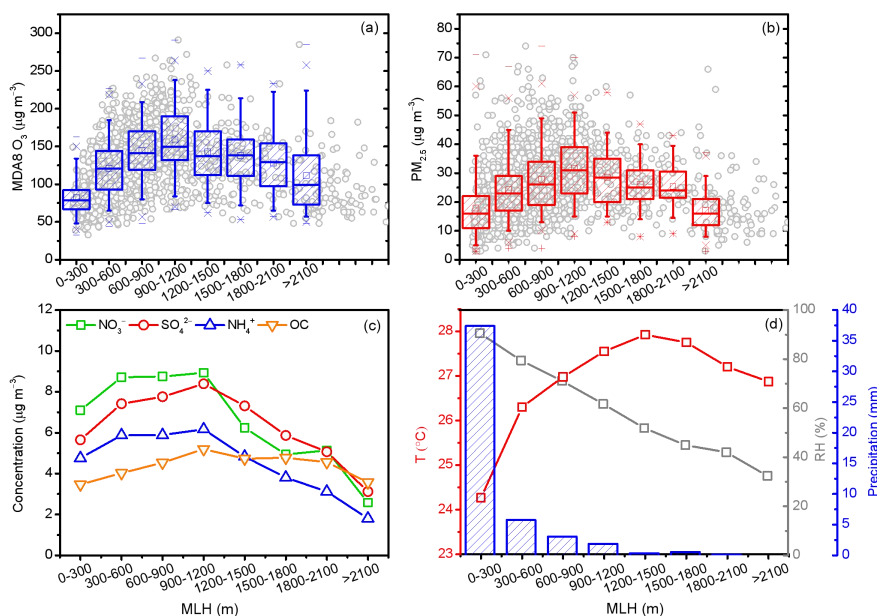
173

174 **Figure 3.** The variation characteristics of (a) MDA8 O₃, (b) PM₂.₅, (c) major secondary aerosol species,

175 and (d) meteorological parameters in different MLH conditions. Box plots in (a) and (b) show the inter

176 quartile range (the distance between the bottom and the top of the box), median (the band inside the

177 box), and 95 % confidence interval (whiskers above and below the box) of the data.

178 To quantify the effect of MLH on near-ground O₃ concentrations, relationships between MLH and

179 MDA8 O₃ were analyzed (Figure 3a). Here we used a data binning method to remove the expected

180 day-to-day atmospheric variability from sampling uncertainty (Dian et al., 2010), which has been

181 applied elsewhere (Lou et al., 2019). The MLH was grouped into 8 classes with 300 m width: 0–300,

182 300–600, 600–900, 900–1200, 1200–1500, 1500–1800, 1800–2100 and > 2100 m. It was found that

183 MDA8 O₃ concentration initially increased and reached the maximum (158.47±44.54 μg m⁻³) when

184 MLH at around 900–1200 m, then turned to decrease with further development of MLH. This nonlinear

185 relationship between MDA8 O₃ and MLH was is inconsistent with previous studies, in which high O₃

186 concentrations corresponded to a low boundary layer height (NASTRO, 2000), but consistent with the

187 results conducted by Zhao et al. (2019) and Reddy et al. (2012). The work by Zhao et al. (2019) found

188 that O₃ concentration was the highest at medium boundary layer heights (1200–1500 m) in

189 Shijiazhuang, China. In India, days of higher O₃ concentrations were also associated with higher

190 boundary layer height (Reddy et al., 2012).

191 This relationship observed between MDA8 O₃ and MLH can be explained by two dominant

192 processes: vertical transport or photochemical formation. Previous works have shown that higher

193 height of mixing layer can lead to the mixing of near surface air with the O₃ rich air aloft, resulting in

194 the observed enhancements in surface O₃ concentration (Reddy et al., 2012). Besides, the evolution of

195 mixing layer were strongly associated with the change of other meteorological conditions, such as air

196 temperature, RH and precipitation. The increase of MLH often coincided with higher air

197 temperature, lower RH, and less precipitation (Figure 3d), which were more conducive to O₃

198 production (Ma et al., 2021; Haman et al., 2014; Xu et al., 2018). Under this meteorological condition,

199 the photochemical formation of O₃ was more intense, and exceeded the influence of vertical dilution.

200 As shown in Figure 4a–b, as the MLH fixed, MDA8 O₃ concentration climbed up with increase in

201 temperature but decrease in RH levels. Possible reasons for these results could be: (1) the increase in

202 RH can contribute to the depletion of O₃, and lead to weakened O₃ related photochemical reaction (Ma

203 et al., 2021; Yu, 2019); and (2) the rise of temperature can accelerate the emission rate of gaseous

204   precursors, such as biogenic VOCs and soil NO_X (Dang et al., 2021; Porter and Heald, 2019), and also

205   stimulate the photochemical reaction rate in the generation of O_3 (Ma et al., 2021). In comparison, the

206   effects of precipitation and WS to the initial growth of MAD8 O_3 were inapparent in this work.
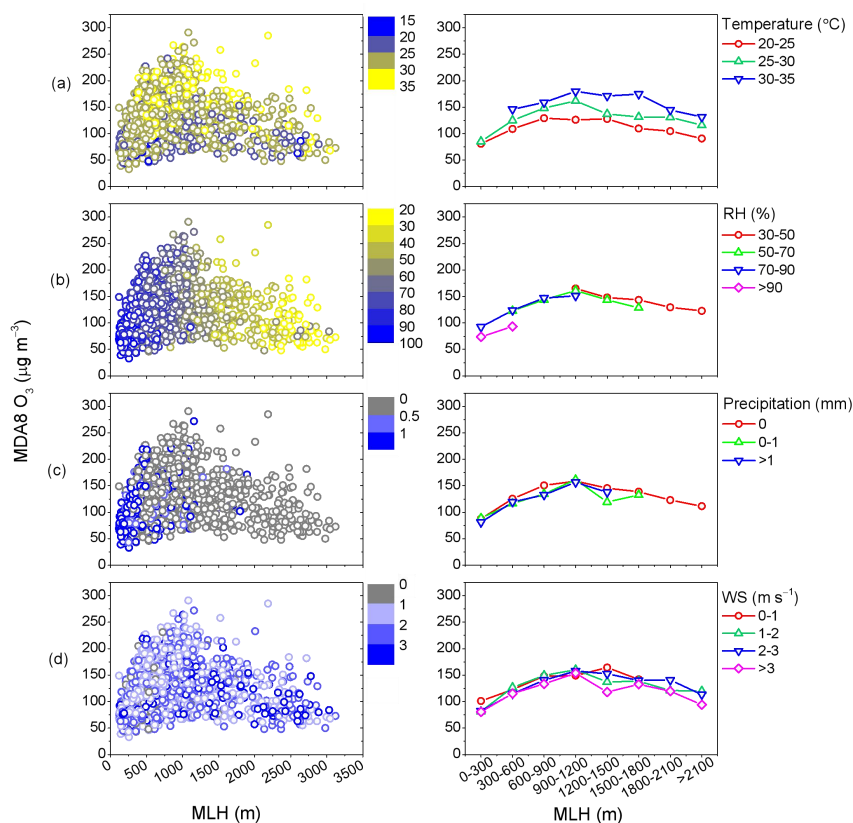
208   **Figure 4.** The distribution characteristics of the MDA8 O_3 concentrations with the evolution of MLH

209   under different (a) temperature, (b) RH, (c) precipitation, and (d) WS conditions.

210   **3.3 Evolution of PM$_{2.5}$ and its secondary compositions with mixing layer meteorology**

211   The concentration distribution of surface PM$_{2.5}$ in different MLH bins has been shown in Figure

212   3b. Interestingly, PM$_{2.5}$ showed similar change profile as MDA8 O_3, which initially increased and then

213   declined along with the growth of MLH. PM$_{2.5}$ concentration reached the maximum of 31.65 μg m^{-3}

214   when MLH fell in the range of 900–1200 m, and the concentration has increased by 1.51 μg m^{-3}

215   through the rise phase for the variation of 100 m MLH. This phenomenon was quite different with the

216   results in cold seasons (Pan et al., 2019; Du et al., 2013; Murthy et al., 2020). The narrowing of mixing

217   layer can inhibit the vertical dilution and dispersion of pollutants and make pollutants accumulate

218   locally, MLH thus has been illustrated as the key factor to aggravate the haze events in large cities of

219   China in winter. However, the response of $PM_{2.5}$ concentration to MLH is not only determined by the

220   vertical stratification of the mixing layer, but also by local sources, secondary chemical formation, wet

221   deposition, and the wind field. Previous works also fund that the statistical relationship between the

222   daily MLH and air pollution levels can become uncorrelated or even positive (Lu et al., 2019; Geiß et

223   al., 2017). Distinct correlations between primary, secondary pollutants and MLH during summer and

224   winter observations were observed (Geiß et al., 2017). The work by Geiß et al. (2017) found little

225   correlation between MLH and $PM_{2.5}$ in Berlin during hot seasons. The observation in Shanghai found

226   that the $PM_{2.5}$ diurnal variation presented different patterns in summer and winter (Pan et al., 2019).

227   The $PM_{2.5}$ diurnal peaks in winter well corresponded to the low mixing layer conditions (200-300 m),

228   while in summer, the diurnal $PM_{2.5}$ concentration peaked in medium mixing layer condition (1000 m).

229   The work by Miao et al. (2021) found that the summertime concurring $PM_{2.5}$ and O_3 pollution in

230   Shanghai usually occurred on the days with deep afternoon planetary boundary layer. Based on the

231   summertime soundings from China for the period from 2014 to 2017, Lou et al. (2019) found that the

232   relationships between the boundary layer height (BLH) and $PM_{2.5}$ were variable under different BLH

233   regimes, and the aerosol loadings increases with the increasing BLH for the Stable Boundary Layer.

234   Noted that in this work there were still some extreme high $PM_{2.5}$ values under low MLH condition as

235   shown in Figure 3b, and this phenomenon will be discussed in the following part when exploring the

236   effect of precipitation.

237   The response of $PM_{2.5}$ concentrations to mixing layer structure was the net effect of the changes in

238    $PM_{2.5}$ major chemical components, such as SO_4^{2-}, NO_3^-, NH_4^+, and OC. Interestingly, the change

239   profiles of these $PM_{2.5}$ components to the evolution of MLH were different. As shown in Figure 3c,

240   SO_4^{2-} and OC both increased and reached the maximum values when MLH in the range of 900–1200m,

241   with the values of 8.39±3.03 μg m^{-3} and 5.20±1.90 μg m^{-3}, respectively. However, NO_3^- and NH_4^+

242   slightly increased when MLH lower than 600m, and kept almost stable when MLH in the range of

243   600–1200m, then significantly decreased with further increase of MLH. The increasing trend (MLH <

244   1200m) of $PM_{2.5}$ was mainly attributed to the enhancement of SO_4^{2-} and OC. The mass ratio of SO_4^{2-} to

245   NO_3^- gradually increased along with the development of mixing layer (Figure S2). When MLH higher

246   than 1200m, SO_4^{2-} surpassed NO_3^- and became the dominant $PM_{2.5}$ component. Changes in NH_4^+ were

247 a consequence of the changes in SO_4^{2-} and NO_3^-. The difference in the relationships between these

248 aerosol species and MLH reflected the intrinsic complexity mechanisms of $PM_{2.5}$ formation, which

249 were probably related to other meteorological parameters, such as temperature, RH, precipitation and

250 WS. In order to understand how the other meteorological factors impacted the relationship between

251 MLH and $PM_{2.5}$, we demonstrated the statistics on the concentration distribution of $PM_{2.5}$ and its

252 dominant components with the increase of MLH under different RH, temperature, precipitation and

253 WS conditions in Figure 5 and Figure 7.

254
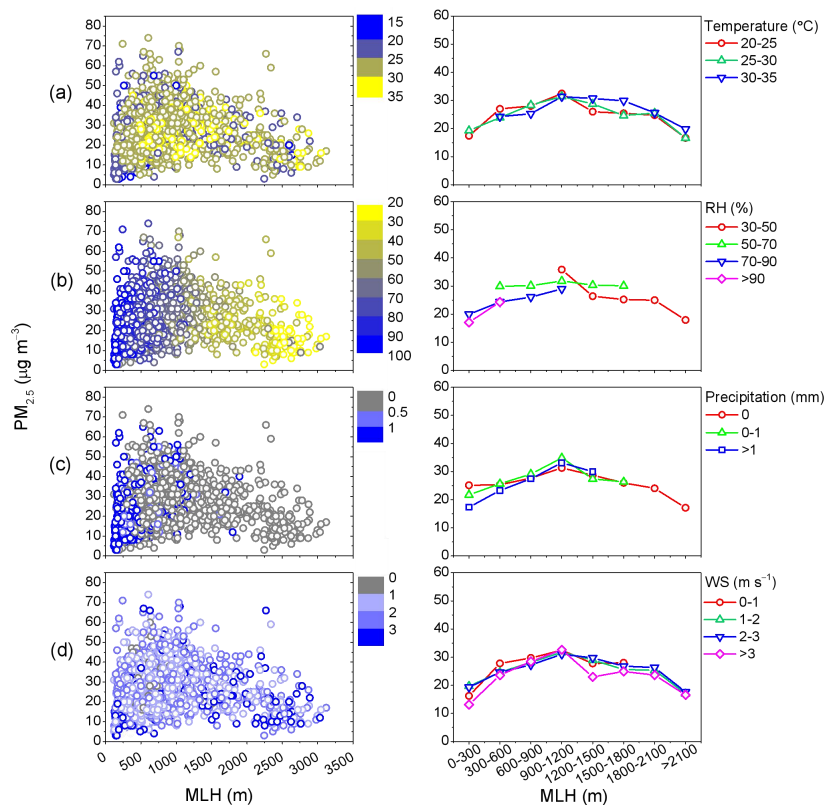
Figure 5. The distribution characteristics of the $PM_{2.5}$ concentrations with the evolution of MLH under

256 different (a) temperature, (b) RH, (c) precipitation, and (d) WS conditions.

257   Temperature is not only essential to the secondary chemical reaction of trace gases, but also the

258 gas–particle partitioning of volatile $PM_{2.5}$ species. The response of $PM_{2.5}$ and its dominant components

259 to MLH followed similar change characteristics under different temperature conditions, all increasing

260 with the development of mixing layer when MLH lower than 1200m. The response of $PM_{2.5}$ to

261 temperature was largely the result of competing changes in NO_3^- and SO_4^{2-} concentrations with a

262   smaller role played by organics (Figure 7). Specifically, as the MLH fixed, SO_4^{2-} concentration

263   climbed up with increasing temperature level, while the concentration of NO_3^- declined when

264   temperature kept going up. Higher temperature may lead to rapid oxidation of SO_2 to SO_4^{2-}. However,

265   the partitioning of semi-volatile nitrate is temperature-dependent. Higher temperature prompts the

266   partitioning of nitrate to HNO_3, thus nitrate tends to exit in the particulate phase, resulting in a

267   significant decrease in NO_3^- and NH_4^+ concentrations.

268   The response of $PM_{2.5}$ and its dominant components to the evolution of mixing layer was more

269   sensitive to RH, and distinct distribution characteristics under different RH ranges have been observed

270   in Figure 5 (b) and Figure 7 (b). When MLH fell in the range of 600–900 m, the concentration of $PM_{2.5}$

271   and its major components mostly decreased with RH elevating from 50–70 % to 70–90 %. Previous

272   works have shown that when RH higher than 60%, local humidity-related physicochemical processes

273   play important roles in transforming the gases to aerosols (Wang et al., 2022d; Liu et al., 2020). We

274   considered that the RH range from 50% to 70% was more beneficial to the aqueous chemical

275   production of major $PM_{2.5}$ components, then led to the increase of $PM_{2.5}$ concentration. It is worth

276   noting that as MLH fixed (0 < MLH < 300 m), when RH rose from 70–90 % to > 90 %, the

277   concentration of $PM_{2.5}$ and its major components severely dropped, which was probably related to the

278   fast hygroscopic growth and enhanced wet deposition processes.
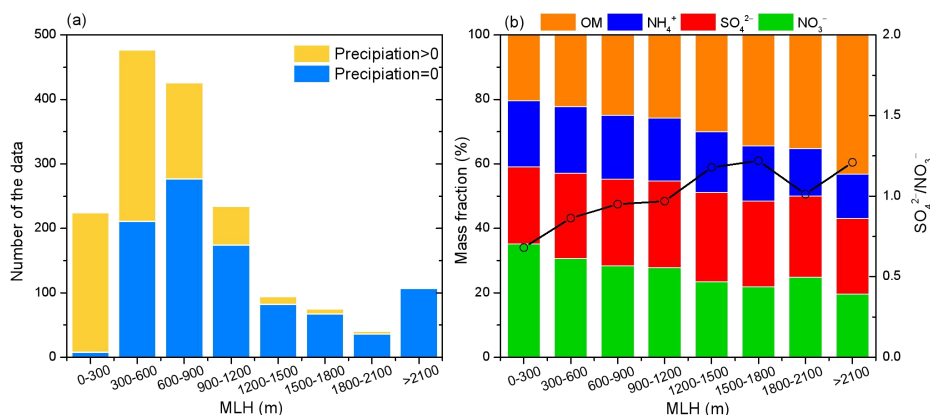
279

280   **Figure 6.** (a) The number distributions of the data when the daily precipitation larger than 0 mm or

281   equal to 0 mm along with the evolution of MLH. (b) The mass fractions of major $PM_{2.5}$ components

282   and the mass ratio of SO_4^{2-} to NO_3^- along with the evolution of MLH when the daily precipitation

283   equal to 0 mm.

284   All aerosol species have wet deposition as a major sink, so precipitation is expected to have

285   significant effects on $PM_{2.5}$ concentrations. As shown in Figure 5 (c), changes in the concentrations of

286    $PM_{2.5}$ was sensitive to the rain events. When MLH fell in the range of 0–300 m, the concentration of

287    $PM_{2.5}$ obvious decreased during rainfall period. Interestingly, when no rainfall occurred, even though

288    $PM_{2.5}$ concentration kept stable under low MLH condition, the response of $PM_{2.5}$ concentrations to

289   MLH still followed upward trend with MLH increasing from 300–600 to 900–1200 m. The observed

290    $PM_{2.5}$ concentrations under moderate MLH condition (900–1200 m) was around 31.34 μg m^{-3}, which

291   was still about six times higher than the WHO's $PM_{2.5}$ guideline value (5 μg m^{-3}, World Health

292   Organization, 2021). As for specific aerosol species, NO_3^- and NH_4^+ concentration showed two obvious

293   peaks, with one in the range of 0–300 m, and the other in 900–1200 m. Under low MLH condition, the

294   concentrations of NO_3^- and NH_4^+ were high, with NO_3^- as the dominant species in $PM_{2.5}$ as shown in

295   Figure 6 (b). With the growth of MLH, NO_3^- and NH_4^+ initially decreased, but turned to increase again

296   when MLH in the range of 900–1200 m. As for SO_4^{2-} and OM (OC×1.6), the concentrations obvious

297   increased with the elevation of MLH and has exceeded that of NO_3^- when MLH higher than 1200 m.

298   As shown in Figure 6 (a), low mixing layer generally accompanied with cloudy and rainy conditions

299   during summertime in the NCP in 2021, and only small fraction of days without rainfall has been

300   captured during this period. Therefore, despite some high $PM_{2.5}$ or major aerosol species values have

301   been witnessed under low MLH condition, the overall trend in Figure 3 (b) was still upwards along

302   with the growth of mixing layer (MLH < 1200 m). The upward trend under medium MLH condition

303   indicated that the particle removal by precipitation was potentially important but not the only

304   controlling factor driving this growing trend, and the enhancement of secondary aerosol formation due

305   to appropriate chemical reaction environment should be considered.

306   WS can represent the atmospheric dissipation potential in the horizontal directions (Zhu et al.,

307   2018). Low WS generally suggested weak pressure gradients and potentially a more favorable

308   meteorological condition for $PM_{2.5}$ enhancement (Ma et al., 2021). As expected, the concentrations of

309    $PM_{2.5}$ and its aerosol species gradually decreased with the increase of WS. However, the response of

310   these air pollutants to MLH followed similar upward trends under different WS conditions (MLH <

311   1200 m). This indicated that the elevation of $PM_{2.5}$ and its aerosol species along with the evolution of

312   mixing layer (MLH < 1200 m) was not attributed to the effect of horizontal diffusion.

313
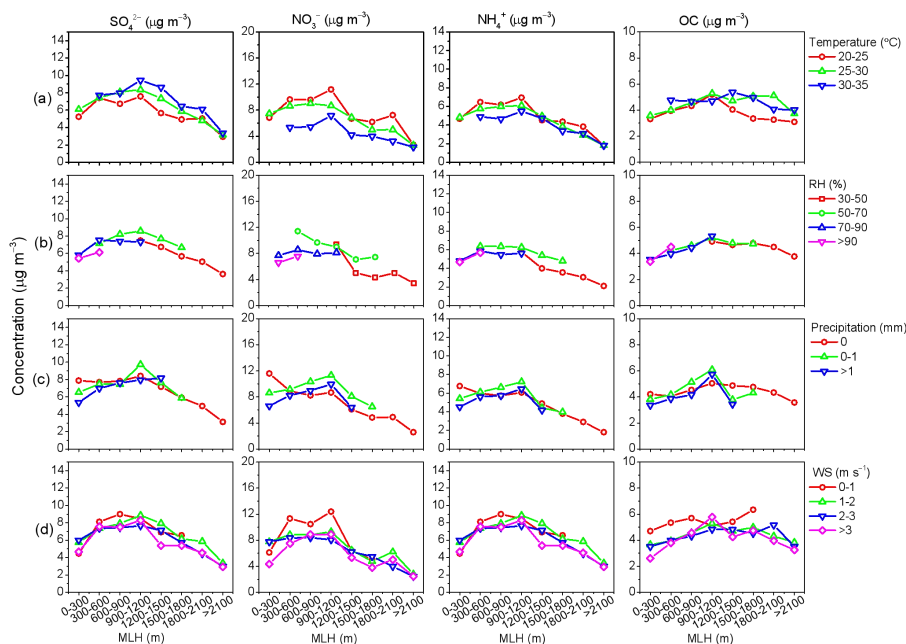
Figure 7. The distribution characteristics of NO_3^-, SO_4^{2-}, NH_4^+, and OC concentrations with the

evolution of MLH under different (a) temperature, (b) RH, (c) precipitation, and (d) WS conditions.

3.4 Impact of atmospheric oxidation capacity on surface PM$_{2.5}$ change profile

The above analysis shows that MDA8 O_3 and PM$_{2.5}$ concentrations were closely related to the

evolution of BLH. The increasing trend of PM$_{2.5}$ concentration with the development of mixing layer

under medium MLH condition discussed before indicated that the evolution of mixing layer was not a

simple physical dilution process, and its influence on the enhanced secondary photochemical formation

should be considered as well. Interestingly, in this work we found three concurring PM$_{2.5}$ and MDA8

O_3 pollution cases along with the development of mixing layer: June 10–13, June 26–29, and July 9–11.

Figure 8 demonstrated a case study to illustrate the detailed regional change characteristics of MLH,

MDA8 O_3, PM$_{2.5}$ and its chemical compositions from 10 to 13 on June 2021. It was found that during

this period, MLH evolved substantially, with the daily height varying from 300–600 m to 900–1500 m.

Concurrently, PM$_{2.5}$ and MDA8 O_3 concentrations also increased, and the areas of highest PM$_{2.5}$

concentrations coincided well with those of highest MDA8 O_3 concentrations. In general, most cities

during this period were in the steady conditions with high temperature and low humidity. The vertical

profiles of O_3 concentration (24-h averaged) and extinction coefficient in TangS, BeiJ, and SJZ (Figure

330   9) indicated that the elevation of O_3 during this period was mainly resulted from the vertical transport

331   from higher mixing layer, while the increase of $PM_{2.5}$ was not attributed to regional transport, but

332   probably enhanced O_3 related secondary aerosol formation. It was found that the increase of $PM_{2.5}$ was

333   mainly due to the enhanced formation of SO_4^{2-} and OC. The chemical composition of $PM_{2.5}$ changed

334   substantially in the NCP during this observation period: NO_3^- decreased with the development of

335   mixing layer in June 11 and 12, and the areas dominated by NO_3^- gradually withdrew, while the

336   contribution of SO_4^{2-} and OC in $PM_{2.5}$ significantly increased.
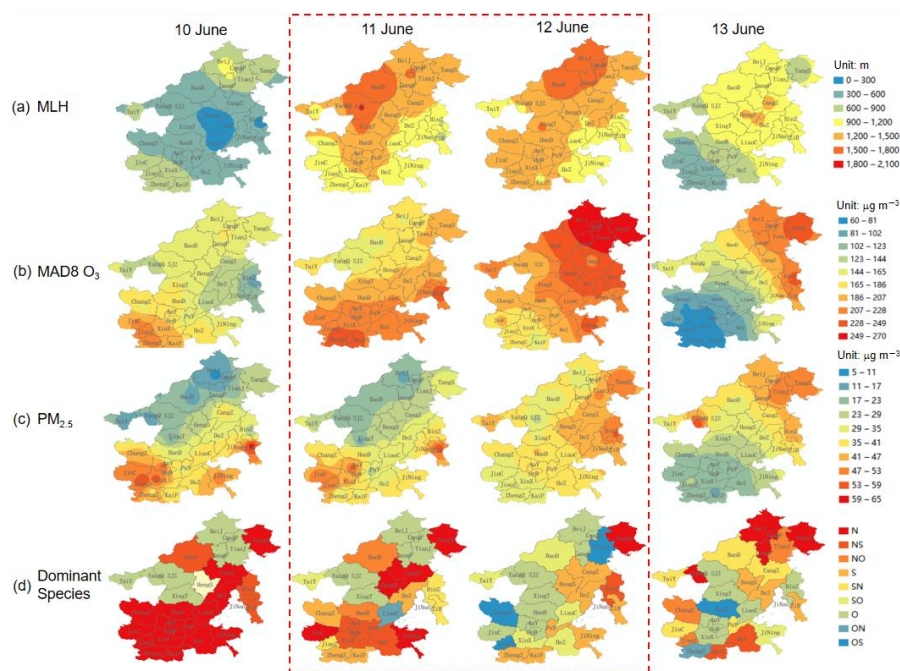
337

338   **Figure 8.** The spatial distribution of (a) MLH, (b) MDA8 O_3, (c) $PM_{2.5}$, and (d) the dominant $PM_{2.5}$

339   chemical component (N: NO_3^- dominant, NS: NO_3^- and SO_4^{2-} dominant, NO: NO_3^- and OM dominant,

340   S: SO_4^{2-} dominant, SN: SO_4^{2-} and NO_3^- dominant, SO: SO_4^{2-} and OM dominant, O: OM dominant, ON:

341   OM and NO_3^- dominant, OS: OM and SO_4^{2-} dominant) from June 10 to 13, 2021. The dominant $PM_{2.5}$

342   chemical component type was identified as the method proposed by Wang et al. (2022b).
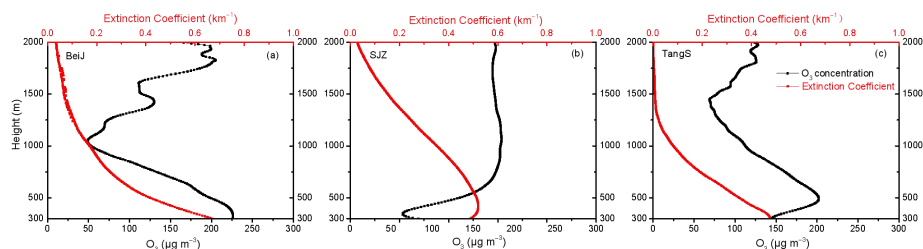
Figure 9. The vertical profiles of O_3 concentration (24-h averaged) and extinction coefficient in (a)

BeiJ, (b) SJZ, and (c) TangS in June 12, 2021
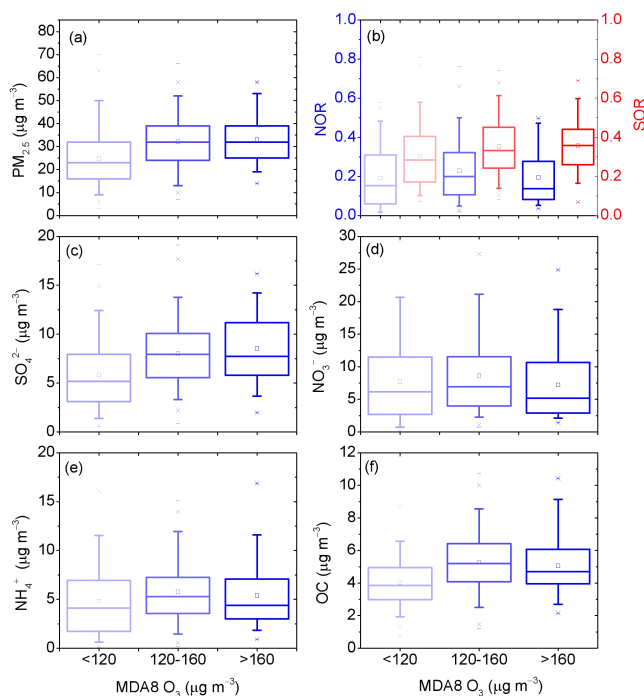
Figure 10. Box plots showing the statistics of (a) $PM_{2.5}$, (b) NOR and SOR, (c) SO_4^{2-}, (d) NO_3^-, (e)

NH_4^+, and (f) OC for different MDA8 O_3 conditions (< 120 μg m^{-3}, 120–160 μg m^{-3}, > 160 μg m^{-3}).

The distance between the bottom and the top of the box reflects the inter quartile range; the line and

square in between are the median and mean values, respectively. The whiskers above and below the

box refer the 95 % confidence interval of the data. Note that rainy days were excluded.

Figure 10 displays the box-and-whisker plots of $PM_{2.5}$ and its major components for different

MDA8 O_3 conditions. To isolate the impacts of precipitation on $PM_{2.5}$ concentration, these rainy days

when the daily rainfall amount greater than 0 mm were excluded in this section. Here the concentration

355 of PM$_{2.5}$ was found to increase synchronously with elevated MDA8 O$_3$ concentration, especially when

356 MDA8 O$_3$ increased from < 120 to 120–160 μg m^{-3}. This summertime collaborative growth process of

357 PM$_{2.5}$-O$_3$ has also been observed in other works (Wang et al., 2022a; Wu et al., 2022). It's noted that

358 the elevation of PM$_{2.5}$ was mainly due to the changes in SO$_4^{2-}$ and OC, which was consistent with the

359 conclusion discussed before. With elevated MDA8 O$_3$ concentration, the oxidation ratio of sulfate

360 (SOR, the molar ratio of sulfate to the sum of sulfate and SO$_2$) significantly increased, which indicated

361 the strong formation of secondary SO$_4^{2-}$ promoted by high atmospheric oxidation capacity. However,

362 the oxidation ratio of nitrate (NOR, the molar ratio of nitrate to the sum of nitrate and NO$_2$) turned to

363 decreased when MDA8 O$_3$ > 160 μg m^{-3}, demonstrating a more significant role of partitioning process

364 between gas and aerosol than the atmospheric oxidation process under this stage. As the MLH fixed

365 (900 m < MLH < 1200 m), SO$_4^{2-}$ concentration climbed up with enhanced MDA8 O$_3$ concentration,

366 while the concentration of NO$_3^-$ declined (Figure S3). This result further demonstrated the conclusion

367 discussed above: the formation of SO$_4^{2-}$ and OC was closely associated with the enhanced MDA8 O$_3$

368 concentration, while the change characteristics of NO$_3^-$ was mainly determined by the partitioning

369 process between gas and aerosol.

370   To verify the potential impact of photochemical oxidation to the increase of PM$_{2.5}$ concentration

371 with mixing layer development, the changes in PM$_{2.5}$ and MDA8 O$_3$ along with the increase of MLH

372 were quantified in the "2+26" cities in the NCP. Linear regression equations between air pollutants and

373 MLH were fitted during the initial increasing stage (300 < MLH < 1200 m) and their slopes were given

374 in Figure 11. The slopes indicated the rates of the maximum changes in air pollutant concentration for a

375 unit change in MLH (100 m). The slopes of PM$_{2.5}$ and O$_3$ were expressed as ΔPM$_{2.5}$ and ΔO$_3$ (μg m^{-3}

376 (100) m^{-1}). It was found that ΔPM$_{2.5}$ was closely related to ΔO$_3$ (R^2=0.60), and obvious spatial

377 difference in ΔPM$_{2.5}$ and ΔO$_3$ was witnessed in the NCP during the observation period. ΔPM$_{2.5}$ and ΔO$_3$

378 both showed high values in TianJ, YangQ, and LangF, with values of 3.43 and 19.56 μg m^{-3} (100) m^{-1}

379 in TianJ, 7.56 and 18.00 μg m^{-3} (100) m^{-1} in YangQ, and 5.75 and 17.85 μg m^{-3} (100) m^{-1} in LangF,

380 respectively. Comparing with these cities, ΔPM$_{2.5}$ and ΔO$_3$ were lowest in HeB, with the value of 1.80

381 and −2.02 μg m^{-3} (100) m^{-1}, respectively, which implied that the secondary formation here was weak

382 and the surface PM$_{2.5}$ change characteristic was dominantly controlled by local emissions or vertical

383 diffusion effect.

384   Comparing with winter, the photochemistry in summer is quite active due to the strong solar

385   radiation. Even though deep MLH prefers to the dilution of air pollutants, higher MLH can also

386   promote secondary chemical feedback through enhancing the availability of atmospheric oxidation

387   capacity (such as changes in O_3) along with appropriate meteorological condition. This conclusion

388   corresponded well to the finding based on chemical transport model (Dai et al., 2023), which proposed

389   strong chemical production of secondary aerosols when planetary boundary layer height was about

390   946.1m on O_3–$PM_{2.5}$ co-pollution days. The strong chemical productions in the oxidative atmosphere at

391   medium MLH condition may overcome the dilution effect on $PM_{2.5}$ induced by mixing layer

392   development, leading to higher $PM_{2.5}$ level at the ground level.
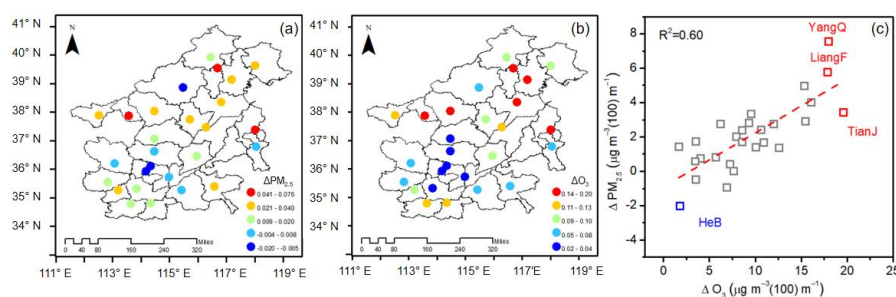
393

394   **Figure 11.** The spatial distribution of (a) $\Delta PM_{2.5}$ and (b) ΔO_3. (c) The relationships between $\Delta PM_{2.5}$ and

395   ΔO_3 in the NCP during summertime. The corresponding correlation coefficients (R^2) was given at the

396   top of the panel.

397   **4 Conclusions**

398   Mixing layer height (MLH) was generally considered as a critical physical parameter in

399   atmospheric environmental evaluation. It is assumed that extended mixing layer may lead to the

400   dilution of air pollutants and thus tend to decrease surface concentrations. Several publications have

401   indeed reported such anti-correlations in cold seasons. However, the understanding of the interaction

402   between near surface O_3 and $PM_{2.5}$ (including its major components) along with the evolution of

403   mixing layer during warm seasons remained poor. Furthermore, previous observational studies were

404   mostly limited to a specific city. This paper is devoted to these topics by examining the response of

405   MDA8 O_3, $PM_{2.5}$, and its major components to the changes in mixing layer meteorology in the North

406   China Plain (NCP) during summertime. We showed that MDA8 O_3 initially increased and then

407   decreased with the growth of MLH. The maximum turning point of MLH was around 900–1200 m. As

408   for near-ground $PM_{2.5}$, similar non-linear change profile was found, with the maximum value of 31.65

409   µg m^{-3} under medium MLH condition (900–1200 m), which was quite different from the results

410   conducted in cold seasons. Compared with winter, the occurrence of low MLH during summertime in

411   the NCP was mostly accompanied with cloudy or rainy conditions, which promoted wet deposition and

412   led to low concentrations of $PM_{2.5}$ at the ground level. Under medium MLH condition, strong chemical

413   productions of SO_4^{2-} and OC occurred along with appropriate mixing layer meteorology, where RH

414   was around 50−70 %, and the availability of atmospheric oxidants (i.e., O_3) increased. The strong

415   chemical productions at medium MLH conditions may offset the diffusion effect on $PM_{2.5}$ induced by

416   mixing layer development, resulting in higher $PM_{2.5}$ levels. The chemical characteristics of $PM_{2.5}$

417   significantly changed along with the growth of MLH. The composited concentration of NO_3^- was the

418   highest under low MLH condition, while the composited concentrations of SO_4^{2-} and OC obviously

419   increased under medium MLH condition. Temperature was the key factor controlling the competing

420   changes in NO_3^- and SO_4^{2-} concentrations in $PM_{2.5}$. We conclude that the MLH can be an indicator of

421   air pollutants in cold seasons, but the correlation between MLH and air pollutants, such as O_3 and

422    $PM_{2.5}$, should be treated with care in hot seasons. At least for the observation period in the NCP this

423   was not the case. Although several studies have examined the change characteristics of MLH and its

424   influence on ground-level O_3 and $PM_{2.5}$, it remains challenging to elucidate the mechanism underlying

425   the complex relationships. To better understand the complex interactions between MLH, air pollution,

426   and chemical processing, there is a need to have more extended data sets in time and space. Besides,

427   the aids of explicit models should be needed in the future.

428

429   **Data availability.** The data used in this paper can be provided upon request from the corresponding

430   author.

431

432   **Author contributions. J W and J G** conceived the study and designed the experiments. **J W, F C, X**

433   **Y,Y Y, L L and Y X** analyzed the data. **J W** prepared the manuscript and all the coauthors helped

434   improve the manuscript.

435

436   **Competing interests.** The authors declare that they have no conflict of interest.

437

438   **Acknowledgement.** We thank the platform of National Atmospheric Particulate

439   Chemical-Speciation-Network for making the $PM_{2.5}$ chemical composition data available.

440

441   **Financial support.** This work was supported by the National Natural Science Foundation of China (No.

442   42075182), the National research program for key issues in air pollution control (DQGG2021101) and

443   the Central Level, Scientific Research Institutes for Basic R&D Special Fund Business, China (No.

444   2022YSKY-26).

445   **Reference**

446   Cheng, J., Su, J., Cui, T., Li, X., Dong, X., Sun, F., Yang, Y., Tong, D., Zheng, Y., Li, Y., Li, J., Zhang,

447   Q., and He, K.: Dominant role of emission reduction in PM$_{2.5}$ air quality improvement in Beijing

448   during 2013–2017: a model-based decomposition analysis, Atmos. Chem. Phys., 19, 6125-6146,

449   10.5194/acp-19-6125-2019, 2019.

450   Chu, B., Ma, Q., Liu, J., Ma, J., Zhang, P., Chen, T., Feng, Q., Wang, C., Yang, N., Ma, H., Ma, J.,

451   Russell, A. G., and He, H.: Air Pollutant Correlations in China: Secondary Air Pollutant Responses

452   to NOx and SO$_2$ Control, Environ. Sci. Technol. Let., 7, 695-700, 10.1021/acs.estlett.0c00403, 2020.

453   Cohen, A. J., Brauer, M., Burnett, R., Anderson, H. R., Frostad, J., Estep, K., Balakrishnan, K.,

454   Brunekreef, B., Dandona, L., and Dandona, R.: Estimates and 25-year trends of the global burden of

455   disease attributable to ambient air pollution: an analysis of data from the Global Burden of Diseases

456   Study 2015, Lancet, 2017.

457   Dai, H., Liao, H., Li, K., Yue, X., Yang, Y., Zhu, J., Jin, J., Li, B., and Jiang, X.: Composited analyses

458   of the chemical and physical characteristics of co-polluted days by ozone and PM$_{2.5}$ over 2013–2020

459   in the Beijing–Tianjin–Hebei region, Atmos. Chem. Phys., 23, 23-39, 10.5194/acp-23-23-2023,

460   2023.

461   Dang, R., Liao, H., and Fu, Y.: Quantifying the anthropogenic and meteorological influences on

462   summertime surface ozone in China over 2012–2017, Sci. Total. Environ., 754, 142394,

463   10.1016/j.scitotenv.2020.142394, 2021.

464   Dawson, J. P., Adams, P. J., and Pandis, S. N.: Sensitivity of PM$_{2.5}$ to climate in the Eastern US: a

465   modeling case study, Atmos. Chem. Phys., 7, 4295-4309, 10.5194/acp-7-4295-2007, 2007.

466   Dian, J., Seidel, Chi, O., Ao, and, Kun, and Li: Estimating climatological planetary boundary layer

467   heights from radiosonde observations: Comparison of methods and uncertainty analysis, J. Geophys.

468   Res. Atmos., 10.1029/2009JD013680, 2010.

469   Du, C., Liu, S., Yu, X., Li, X., Chen, C., Peng, Y., Dong, Y., Dong, Z., and Wang, F.: Urban boundary

470   layer height characteristics and relationship with particulate matter mass concentrations in Xi'an,

471   Central China, Aerosol Air Qual. Res., 13, 1598-1607, 10.4209/aaqr.2012.10.0274, 2013.

472   Gao, Y. and Ji, H.: Microscopic morphology and seasonal variation of health effect arising from heavy

473   metals in PM$_{2.5}$ and PM$_{10}$: One-year measurement in a densely populated area of urban Beijing,

474   Atmos. Res., 212, 213-226, https://doi.org/10.1016/j.atmosres.2018.04.027, 2018.

475   Geiß, A., Wiegner, M., Bonn, B., Schäfer, K., Forkel, R., von Schneidemesser, E., Münkel, C., Chan, K.

476   L., and Nothard, R.: Mixing layer height as an indicator for urban air quality?, Atmos. Meas. Tech.,

477   10.5194/amt-2017-53, 2017.

478   Haman, C. L., Couzo, E., Flynn, J. H., Vizuete, W., Heffron, B., and Lefer, B. L.: Relationship between

479   boundary layer heights and growth rates with ground-level ozone in Houston, Texas, J. Geophys. Res.

480   Atmos., 119, 6230-6245, 10.1002/2013jd020473, 2014.

481   Hou, P. and Wu, S.: Long-term changes in extreme air pollution meteorology and the implications for

482   air quality, Sci. Rep., 6, 23792, 10.1038/srep23792, 2016.

483   Jiang, N., Li, L., Wang, S., Li, Q., Dong, Z., Duan, S., Zhang, R., and Li, S.: Variation tendency of

484   pollution characterization, sources, and health risks of $PM_{2.5}$-bound polycyclic aromatic

485   hydrocarbons in an emerging megacity in China: Based on three-year data, Atmos. Res., 217, 81-92,

486   2018.

487   Kang, M., Zhang, J., Zhang, H., and Ying, Q.: On the relevancy of observed ozone increase during

488   COVID-19 lockdown to summertime ozone and $PM_{2.5}$ control policies in China, Environ. Sci.

489   Technol. Let., 8, 289-294, 10.1021/acs.estlett.1c00036, 2021.

490   Kong, L., Du, C., Zhanzakova, A., Cheng, T., and Zhang, S.: Trends in heterogeneous aqueous reaction

491   in continuous haze episodes in suburban Shanghai: An in-depth case study, Sci. Total Environ., 634,

492   1192, 10.1016/j.scitotenv.2018.04.086, 2018.

493   Li, J., Cai, J., Zhang, M., Liu, H., Han, X., Cai, X., and Xu, Y.: Model analysis of meteorology and

494   emission impacts on springtime surface ozone in Shandong, Sci. Total. Environ., 771, 144784,

495   https://doi.org/10.1016/j.scitotenv.2020.144784, 2021.

496   Liu, J., Wu, D., Fan, S., Mao, X., and Chen, H.: A one-year, on-line, multi-site observational study on

497   water-soluble inorganic ions in $PM_{2.5}$ over the Pearl River Delta region, China, Sci. Total Environ.,

498   601-602, 1720-1732, https://doi.org/10.1016/j.scitotenv.2017.06.039, 2017a.

499   Liu, P., Ye, C., Xue, C., Zhang, C., Mu, Y., and Sun, X.: Formation mechanisms of atmospheric nitrate

500   and sulfate during the winter haze pollution periods in Beijing: gas-phase, heterogeneous and

501   aqueous-phase chemistry, Atmos. Chem. Phys., 20, 4153-4165, 10.5194/acp-20-4153-2020, 2020.

502   Liu, T., Gong, S., He, J., Yu, M., and Zhao, Q.: Attributions of meteorological and emission factors to

503   the 2015 winter severe haze pollution episodes in China's Jing-Jin-Ji area, Atmos. Chem. Phys., 17,

504   2971-2980, 10.5194/acp-17-2971-2017, 2017b.

505   Lou, M., Guo, J., Wang, L., Xu, H., Chen, D., Miao, Y., Lv, Y., Li, Y., Guo, X., Ma, S., and Li, J.: On

506   the relationship between aerosol and boundary layer height in summer in China under different

507   thermodynamic conditions, Earth Space Sci., 6, 887-901, 10.1029/2019ea000620, 2019.

508   Lu, M., Tang, X., Wang, Z., Wu, L., Chen, X., Liang, S., Zhou, H., Wu, H., Hu, K., Shen, L., Yu, J., and

509   Zhu, J.: Investigating the transport mechanism of $PM_{2.5}$ pollution during January 2014 in Wuhan,

510   Central China, Adv. Atmos. Sci., 36, 1217-1234, 10.1007/s00376-019-8260-5, 2019.

511   Ma, S., Shao, M., Zhang, Y., Dai, Q., and Xie, M.: Sensitivity of $PM_{2.5}$ and O_3 pollution episodes to

512   meteorological factors over the North China Plain, Sci. Total. Environ., 792, 148474,

513   10.1016/j.scitotenv.2021.148474, 2021.

514   Miao, Y., Che, H., Zhang, X., and Liu, S.: Relationship between summertime concurring $PM_{2.5}$ and O_3

515   pollution and boundary layer height differs between Beijing and Shanghai, China, Environ. Pollut.,

516   268, 115775, 10.1016/j.envpol.2020.115775, 2021.

517   Murthy, B. S., Latha, R., Tiwari, A., Rathod, A., Singh, S., and Beig, G.: Impact of mixing layer height

518   on air quality in winter, J. Atmos. Sol.-Terr. Phy., 197, 10.1016/j.jastp.2019.105157, 2020.

519   NASTRO (The North American Research Strategy for Tropospheric Ozone): An assessment of

520   tropospheric ozone pollution: a North American perspective , 2000.

521   Pan, L., Xu, J., Tie, X., Mao, X., Gao, W., and Chang, L.: Long-term measurements of planetary

522   boundary layer height and interactions with $PM_{2.5}$ in Shanghai, China, Atmos. Pollut. Res., 10,

523   989-996, 10.1016/j.apr.2019.01.007, 2019.

524   Pang, N., Gao, J., Che, F., Ma, T., Liu, S., Yang, Y., Zhao, P., Yuan, J., Liu, J., Xu, Z., and Chai, F.:

525   Cause of $PM_{2.5}$ pollution during the 2016–2017 heating season in Beijing, Tianjin, and Langfang,

526   China, J. Environ. Sci. (China), 95, 201-209, 10.1016/j.jes.2020.03.024, 2020.

527   Porter, W. C. and Heald, C. L.: The mechanisms and meteorological drivers of the summertime

528   ozone–temperature relationship, Atmos. Chem. Phys., 19, 13367-13381,

529   10.5194/acp-19-13367-2019, 2019.

530   Reddy, K. K., Naja, M., Ojha, N., Mahesh, P., and Lal, S.: Influences of the boundary layer evolution

531   on surface ozone variations at a tropical rural site in India, J. Earth Syst. Sci., 121, 911-922,

532   10.1007/s12040-012-0200-z, 2012.

533   Seinfeld, J. H. and Pandis, S. N.: Atmospheric Chemistry and Physics: From Air Pollution to Climate

534   Change, . 2nd ed.; J. Wiley: Hoboken, N.J.,, p xxviii, 1203 p., 2006.

535   Steiner, Allison, L., Davis, Adam, J., Sillman, Sanford, Owen, Robert, C., Michalak, and Anna, M.:

536   Observed suppression of ozone formation at extremely high temperatures due to chemical and

537   biophysical feedbacks Proc. Natl. Acad. Sci. U. S. A., 107, 19685–19690, 2010.

538   Stull, R.: An Introduction to Boundary Layer Meteorology, Kluwer Academic Publishers, Dordrecht,

539   the Netherlands, 1988.

540   Wang, F., Wang, W., Wang, Z., Zhang, Z., Feng, Y., Russell, A. G., and Shi, G.: Drivers of $PM_{2.5}$–O_3

541   co-pollution: from the perspective of reactive nitrogen conversion pathways in atmospheric nitrogen

542   cycling, Sci. Bull. (Beijing), 67, 1833-1836, 10.1016/j.scib.2022.08.016, 2022a.

543   Wang, G., Zhang, R., Gomez, M. E., Yang, L., Levy Zamora, M., Hu, M., Lin, Y., Peng, J., Guo, S.,

544   Meng, J., Li, J., Cheng, C., Hu, T., Ren, Y., Wang, Y., Gao, J., Cao, J., An, Z., Zhou, W., Li, G., Wang,

545   J., Tian, P., Marrero-Ortiz, W., Secrest, J., Du, Z., Zheng, J., Shang, D., Zeng, L., Shao, M., Wang,

546   W., Huang, Y., Wang, Y., Zhu, Y., Li, Y., Hu, J., Pan, B., Cai, L., Cheng, Y., Ji, Y., Zhang, F.,

547   Rosenfeld, D., Liss, P. S., Duce, R. A., Kolb, C. E., and Molina, M. J.: Persistent sulfate formation

548   from London Fog to Chinese haze, Proc. Natl. Acad. Sci. U. S. A., 113, 13630-13635,

549   10.1073/pnas.1616540113, 2016.

550   Wang, J., Gao, J., Che, F., Wang, Y., Lin, P., and Zhang, Y.: Dramatic changes in aerosol composition

551   during the 2016–2020 heating seasons in Beijing–Tianjin–Hebei region and its surrounding areas:

552   The role of primary pollutants and secondary aerosol formation, Sci. Total. Environ., 849, 157621,

553   10.1016/j.scitotenv.2022.157621, 2022b.

554   Wang, J., Yang, Y., Jiang, X., Wang, D., Zhong, J., and Wang, Y.: Observational study of the $PM_{2.5}$ and

555   O_3 superposition-composite pollution event during spring 2020 in Beijing associated with the water

556   vapor   conveyor   belt   in   the   northern   hemisphere,   Atmos.   Environ.,   272,

557   10.1016/j.atmosenv.2022.118966, 2022c.

558   Wang, J., Yang, Y., Zhang, X., Liu, H., Che, H., Shen, X., and Wang, Y.: On the influence of

559   atmospheric super-saturation layer on China's heavy haze-fog events, Atmos. Environ., 171, 261-271,

560   https://doi.org/10.1016/j.atmosenv.2017.10.034, 2017.

561   Wang, M., Duan, Y., Xu, W., Wang, Q., Zhang, Z., Yuan, Q., Li, X., Han, S., Tong, H., Huo, J., Chen, J.,

562   Gao, S., Wu, Z., Cui, L., Huang, Y., Xiu, G., Cao, J., Fu, Q., and Lee, S.-c.: Measurement report:

563   Characterisation and sources of the secondary organic carbon in a Chinese megacity over 5 years

564  from 2016 to 2020, Atmos. Chem. Phys., 22, 12789-12802, 10.5194/acp-22-12789-2022, 2022d.

565  Wang, X., Xiang, Y., Liu, W., Lv, L., Dong, Y., Fan, G., Ou, J., and Zhang, T.: Vertical profiles and

566  regional transport of ozone and aerosols in the Yangtze River Delta during the 2016 G20 summit

567  based on multiple lidars, Atmos. Environ., 259, 10.1016/j.atmosenv.2021.118506, 2021.

568  Wen, L., Xue, L., Wang, X., Xu, C., Chen, T., Yang, L., Wang, T., Zhang, Q., and Wang, W.:

569  Summertime fine particulate nitrate pollution in the North China Plain: increasing trends, formation

570  mechanisms and implications for control policy, Atmos. Chem. Phys., 18, 11261-11275,

571  10.5194/acp-18-11261-2018, 2018.

572  World Health Organization. WHO global air quality guidelines: particulate matter ($PM_{2.5}$ and PM_{10}),

573  ozone, nitrogen dioxide, sulfur dioxide and carbon monoxide. Geneva: World Health Organization,

574  2021.

575  Wu, X., Xin, J., Zhang, W., Gao, W., Ma, Y., Ma, Y., Wen, T., Liu, Z., Hu, B., Wang, Y., and Wang, L.:

576  Variation characteristics of air combined pollution in Beijing City, Atmos. Res., 274,

577  10.1016/j.atmosres.2022.106197, 2022.

578  Xu, X., Zhang, H., Lin, W., Wang, Y., Xu, W., and Jia, S.: First simultaneous measurements of

579  peroxyacetyl nitrate (PAN) and ozone at Nam Co in the central Tibetan Plateau: impacts from the

580  PBL evolution and transport processes, Atmos. Chem. Phys., 18, 5199-5217,

581  10.5194/acp-18-5199-2018, 2018.

582  Yu, S.: Fog geoengineering to abate local ozone pollution at ground level by enhancing air moisture,

583  Environ. Chem. Lett., 17, 565-580, 10.1007/s10311-018-0809-5, 2019.

584  Zhang, H., Wang, Y., Hu, J., Ying, Q., and Hu, X.-M.: Relationships between meteorological

585  parameters and criteria air pollutants in three megacities in China, Environmental Research, 140,

586  242-254, https://doi.org/10.1016/j.envres.2015.04.004, 2015a.

587  Zhang, R., Wang, G., Guo, S., Zamora, M. L., Ying, Q., Lin, Y., Wang, W., Hu, M., and Wang, Y.:

588  Formation of urban fine particulate matter, Chem. Rev., 115, 3803-3855,

589  10.1021/acs.chemrev.5b00067, 2015b.

590  Zhang, X., Xiao, X., Wang, F., Brasseur, G., Chen, S., Wang, J., and Gao, M.: Observed sensitivities of

591  $PM_{2.5}$ and O_3 extremes to meteorological conditions in China and implications for the future,

592  Environ. Int., 168, 107428, 10.1016/j.envint.2022.107428, 2022.

593  Zhao, W., Tang, G., Yu, H., Yang, Y., Wang, Y., Wang, L., An, J., Gao, W., Hu, B., Cheng, M., An, X.,

594   Li, X., and Wang, Y.: Evolution of boundary layer ozone in Shijiazhuang, a suburban site on the

595   North China Plain, J. Environ. Sci. (China), 83, 152-160, 10.1016/j.jes.2019.02.016, 2019.

596   Zhu, X., Tang, G., Guo, J., Hu, B., Song, T., Wang, L., Xin, J., Gao, W., Münkel, C., Schäfer, K., Li, X.,

597   and Wang, Y.: Mixing layer height on the North China Plain and meteorological evidence of serious

598   air pollution in southern Hebei, Atmos. Chem. Phys., 18, 4897-4910, 10.5194/acp-18-4897-2018,

599   2018.